PCCP

Accepted Manuscript

ROYAL SOCIETY OF CHEMISTRY

www.rsc.org/pccp

Does Hooke's law work in helical nanosprings?

Sudong Ben[1], Junhua Zhao[1*], Timon Rabczuk[2]

[1]*Jiangsu Key Laboratory of Advanced Manufacturing Equipment and Technology of Food, Jiangnan University, 214122, Wuxi, China*

[2]*Institute of Structural Mechanics, Bauhaus-University Weimar, 99423 Weimar, Germany*

Abstract

Hooke's law is a principle of physics that states that the force needed to extend a spring by some distance is proportional to that distance. The law is always valid for an initial portion of the elastic range for nearly all helical macrosprings. Here we report the sharply nonlinear force-displacement relation of tightly wound helical carbon nanotubes at even small displacement via a molecular mechanics model. We demonstrate that the van der Waals (vdW) interaction between the intertube walls dominates the nonlinear relation based on our analytical expressions. This study provides physical insights into the origins of huge nonlinearity of the helical nanosprings.

Keywords: Hooke's law, helical carbon nanotubes, van der Waals interaction.

* Corresponding author. Tel: +86 182 0617 7312
Email address: (JZ) junhua.zhao@163.com

1. Introduction

Hooke's law is always valid for an initial portion of the elastic range for nearly all helical macrosprings in practical applications, which means that $F = -k\delta$, where k is a constant factor characteristic of the spring's stiffness, F is the force and δ is the distance [1]. However, the property of Hooke's law may be not correct for some special helical nanosprings. In this paper, the sharply nonlinear force-displacement relation is occurred at even small displacement via a molecular mechanics model, when the tightly helical carbon tubes (CNTs) (see Fig. 1) are subjected to tensile loading. The helical CNTs (or so-called carbon nanocoils (CNCs)) have been synthesized and studied [2-8]. Based on the observations from high-resolution electron microscopy and electron diffraction [2,3], the atomic models of single-strand CNCs can be constructed by incorporating a specific group of defects, such as the pentagon-heptagon or pentagon-octagon defects [6,8], to coil a straight CNT into jointed-segments helix. Due to their unique helical structures, CNCs exhibit some special electronic, mechanical, thermal, and magnetic properties and possess significant potentials to make resonators, nanosprings, electromagnetic wave absorbers, etc [4-9]. Volodin et al. [10] reported the elastic properties of CNCs as measured with force modulation microscopy. Hayashida et al. [11] revealed that the electric conductivity of the CNCs ranges from 107 to 180 s/cm. Akitaet al. [12] found that CNCs could be semimetal by tight-binding (TB) calculations. Chen et al. [13] measured the mechanical property of a CNC and obtained the spring constant of 0.12 N/m under a low strain. Recently, Wu et al. [14,15] have reported the high energy absorbing capacity of CNCs using molecular dynamics (MD) simulations. However, the softly helical CNTs only considered in all above experiments and the quantitative relation between the force and the distance for tightly helical CNTs are not clear yet.

In this paper, we develop a nonlinear theoretical model to obtain the analytical force-displacement relation of both tightly and softly helical CNTs based on the Chang's stick-spiral model [16,17] by incorporating the Morse type potential [18,19].

2. Analytical force-displacement relation of both tightly and softly helical CNTs

The geometry of a helical CNT (see Fig. 1b) is described as follows:

$$\begin{cases} x = R\cos\alpha \\ y = R\sin\alpha \\ z = \dfrac{h+2r_0}{2\pi}\alpha \end{cases},$$

where R is the helical radius, r_0 is the radius of the CNT, α is the parametric angle, and h is the helix pitch between intertube walls.

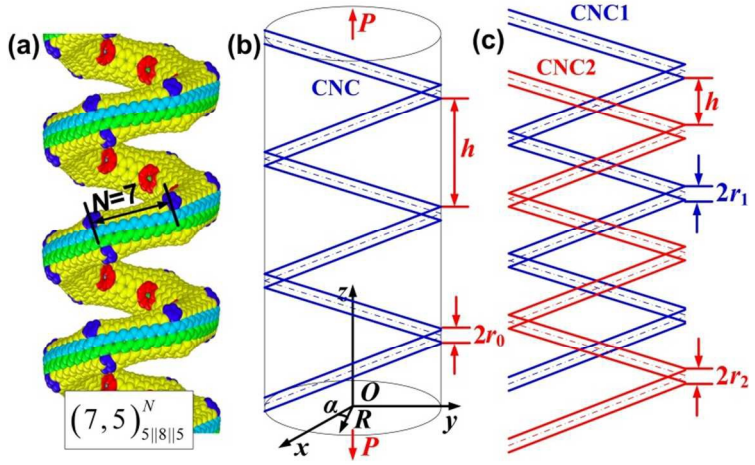

Fig.1 (a) The atomic configuration of a CNC [14]; (b) the geometry and the coordinate of CNC; (c) The geometry of two-strand CNCs.

To show the difference between the softly and tightly helical nanosprings, we use four kinds of models to characterize their force-displacement relation: an elastic model without vdW

interaction, an elastic model with vdW interaction, a nonlinear model without vdW interaction and a nonlinear model with vdW interaction.

It should be stressed that the definition of the tightly and softly helical CNTs is determined by the effect of the vdW force. In this paper, the vdW force is close to zero when the value h is up to 10 Å. In this paper, the difference of the softly and tightly helical CNTs is $h \geqslant 10$ Å and $h<10$ Å, respectively.

2.1 The deflection of CNC under tension from an elastic model (without van der Waals)

For softly helical CNTs, the vdW interaction could be neglected due to the weak vdW force [12]. For example, the diameter and the pitch of the softly helical CNTs are measured around 120 nm and 2 μm in previous experiments, respectively [13].

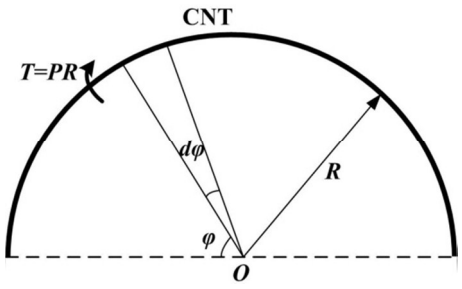

Fig. 2 The half-circle geometry of the helical CNT.

Fig. 2 shows the half-circle geometry of the helical CNT. The bending moment M and the torsion moment T can be expressed as

$$M=PR\sin\varphi-PR\sin\varphi=0, \quad (1)$$

$$T= PR, \quad (2)$$

where P is the tension force (see Fig. 1b).

The actual length of the half-circle length in the three-dimensional (3D) space can be obtained

$$S = \pi\sqrt{R^2 + \left(\frac{h + 2r_0}{2\pi}\right)^2}\ , \tag{3}$$

The total energy of the half-circle length in the 3D space can be obtained

$$U_{beam} = \int_0^{\pi} \frac{(PR)^2}{2GJ} dS = \frac{(PR)^2 \pi}{2GJ}\sqrt{R^2 + \left(\frac{h + 2r_0}{2\pi}\right)^2}\ , \tag{4}$$

where G is the shear modulus and J is the polar moment of inertia.

Based on the energy equivalence, the work $W=P\delta/2$ should be equal to U_{beam} and the $P\sim\delta$ relation can be expressed as

$$P = \frac{GJ}{\pi R^2\sqrt{R^2 + \left(\frac{h + 2r_0}{2\pi}\right)^2}}\delta\ . \tag{5}$$

where G is the shear modulus (here we choose 250 Gpa [17]), and J is the polar moment of inertia (the CNT thickness is chosen as 3.4 Å).

2.2 The deflection of CNC under tension with elastic model (including van der Waals)

As mechanical structures enter the nanoscale regime, the van der Waals (vdW) interaction plays a significant role [20-23]. For the tightly helical CNTs, the vdW interaction should be considered. In previous experiments [24], the tightly helical structures have an outer diameter of about 2 nm and show a pronounced longitudinal periodicity of 1 to 1.2 nm (in which the helix pitch h between intertube walls is close to 3.5 Å). The analysis of the scanning tunneling microscopy data indicates that these tiny, molecular-size coils are made from graphene tubules having the smallest diameter experimentally observed for nanotubes, namely around 0.7 nm [24].

The cohesive energy per unit length between two parallel CNTs (in which their radii are r_1 and r_2, respectively.) can be obtained from our previous work [25]

$$\phi_{cicle} = \pi \in \sigma^6 \rho^2 r_1 r_2 \left(\frac{63}{8}\sigma^6 \int_0^{\pi} \frac{F_5\left[\frac{2\sqrt{a_0 r_1}}{r_1 + a_0}\right]}{\left(r_1 + a_0\right)^{11}} d\theta_2 - 12\int_0^{\pi} \frac{F_2\left[\frac{2\sqrt{a_0 r_1}}{r_1 + a_0}\right]}{\left(r_1 + a_0\right)^{5}} d\theta_2 \right), \tag{6}$$

where $\in$ is the depth of the vdW potential, σ is a parameter that is determined by the equilibrium distance, ρ is the area density (here we homogenize carbon atoms on the CNT), a_0 is the complicated function of the radii (r_1 and r_2) of the two CNTs and h (here h represents the closest distance between the two parallel CNTs edge), F_2 and F_5 are the functions of $2(a_0r_1)/(r_1+a_0)$. The detailed parameters can be seen in reference [25].

Defining $k = \frac{2\sqrt{a}}{1+a} = \frac{2\sqrt{a_0 r_1}}{r_1 + a_0}$,

we can write

$$F_2[k] = \frac{1}{3\left(1-k^2\right)}\left[\left(\frac{4-2k^2}{1-k^2}\right)E(k) - K(k)\right], \tag{7}$$

$$F_5[k] = \frac{1}{315\left(1-k^2\right)^5}\left[\begin{array}{l}\left(128k^8 - 616k^6 + 1179k^4 - 1126k^2 + 563\right)E(k) \\ +\left(-64k^8 + 316k^6 - 624k^4 + 620k^2 - 248\right)K(k)\end{array}\right], \tag{8}$$

where the elliptic integrals are

$$E(k) = \int_0^{\frac{\pi}{2}} \left(1 - k^2 \sin^2 t\right)^{\frac{1}{2}} dt \,, K(k) = \int_0^{\frac{\pi}{2}} \frac{1}{\left(1 - k^2 \sin^2 t\right)^{\frac{1}{2}}} dt \,. \tag{9}$$

Since the function of the above cohesive energy is very complicated, it is not easy to obtain the vdW force q between intertube walls. Here we use the polynomial function to fit Eq. (6) for different CNTs. For example, the cohesive energy of two parallel (10,10) CNTs can be fitted as

$$\phi_{circle}(h)=\frac{408440.7}{h^{12}}+\frac{525.3491}{h^{6}}-\frac{94.4071}{h^{3}}+\frac{0.70549}{h}. \tag{10}$$

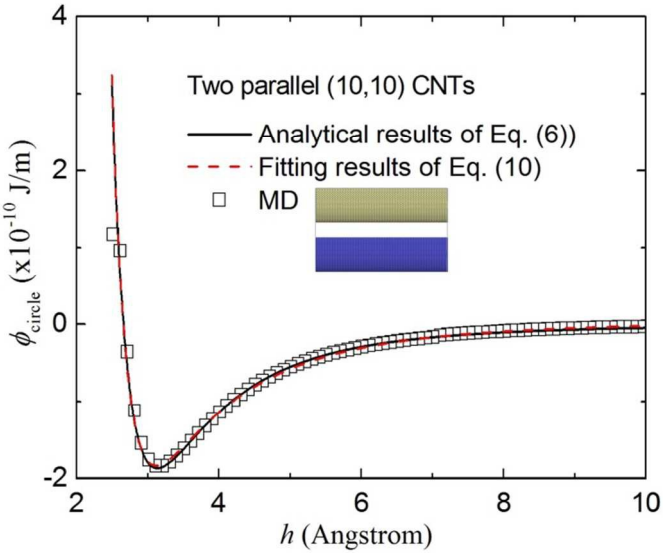

Fig. 3 The cohesive energy between two parallel (10,10) CNTs.

Fig. 3 shows the fitting results by Eq. (10) and our analytical results by Eq. (6). The present fitting results agrees very well with those of Eq. (6) and our full atom MD simulations.

The vdW force q between intertube walls can be expressed by $q=\frac{d\phi_{circle}}{dh}$

$$q=-12\frac{408440.7}{h^{13}}-6\frac{525.3491}{h^{7}}+3\frac{94.4071}{h^{4}}-\frac{0.70549}{h^{2}}, \tag{11}$$

Substituting $\frac{d\phi_{circle}}{dh}=0$ into Eq. (11) gives the equilibrium distance h_0=3.12 (Å). It should be noted that the equilibrium distance h_0 is slightly different for different CNTs, which can be obtained from our previous work [25].

The bending moment M and the torsion moment T can be expressed as

$$dM=qRd\varphi R\sin\varphi,\ M=-qR^2(1-\cos\varphi), \tag{12}$$

$$dT=qRd\varphi R(1-\cos\varphi),\ T=-qR^2(\varphi-\sin\varphi)\ , \tag{13}$$

Based on the elasticity theory, the deflection W can be given

$$EIW''=M\ , \tag{14}$$

where $W=\delta_2=\frac{qR^4\left(2+\frac{\pi^2}{2}\right)}{EI}$ from the boundary condition, in which δ_2 represents the deflection produced by the bending moment M along z direction.

The shear strain γ can be given

$$\gamma=\frac{\tau}{G}=\frac{Tr}{GJ}=\frac{\left(PR-\pi qR^2\right)r}{GJ}, \tag{15}$$

where $\tau=Tr/J$ is the shear stress,

To obtain the relation between δ_1 and T, we have to give the function between δ_1 and γ at first. The work subjected to loading P can be obtained

$$U_{work}=\int P(\delta)d\delta\ . \tag{16}$$

The total energy of the beam without vdW force can be obtained

$$V_{\varepsilon}=\int_{r1}^{r2}2\pi rSdr\int_{0}^{\gamma}\frac{Tr}{J}d\gamma\,, \tag{17}$$

where $V_{\varepsilon}=U_{\text{work}}$.

Substituting Eq. (15) into Eq. (16) and Eq. (17) gives

$$\gamma=r\delta_1/RS. \tag{18}$$

The function between δ_1 and γ can be given

$$\gamma=\frac{r}{\pi R\sqrt{R^2+\left(\frac{h+2r_0}{2\pi}\right)^2}}\delta_1\,. \tag{19}$$

Note that δ_1 of Eq. (19) represents the deflection produced by the torsion strain γ along z direction.

Substituting Eq. (15) into Eq. (19) gives

$$\delta_1=\frac{\left(PR-\pi qR^2\right)\pi R\sqrt{R^2+\left(\frac{h+2r_0}{2\pi}\right)^2}}{GJ}\,. \tag{20}$$

Then we can obtain

$$P=\frac{GJ}{\pi R^2\sqrt{R^2+\left(\frac{h+2r_0}{2\pi}\right)^2}}\delta_1+\pi qR\,. \tag{21}$$

Since the displacement δ is equal to

$$\delta=\delta_1-\delta_2, \tag{22}$$

the relation between the force P and the displacement δ from elastic model with vdW interaction can be obtained

$$P = \frac{GJ}{\pi R^2 \sqrt{R^2 + \left(\frac{h+2r_0}{2\pi}\right)^2}} \left(\delta - \frac{qR^4\left(2+\frac{\pi^2}{2}\right)}{EI} \right) + \pi qR, \tag{23}$$

where q represents the vdW force between intertube walls and can be expressed as $q = \frac{\partial \phi_{cicle}}{\partial h}$, and ϕ_{circle} is the cohesive energy between two parallel CNTs and is a complicated function of h and CNT radii [25].

2.3 The deflection of CNC under tension using nonlinear functions of Morse potentials (without van der Waals)

The CNCs are taken as the linear elastic materials in sections 2.1 and 2.2. To more accurately describe the mechanical behavior under large deformation, the CNCs will be considered as the nonlinear materials in sections 2.3 and 2.4.

The relation between the force P and the displacement δ from nonliear model without vdW interaction can be obtained based on the stick-spiral model by incorporating the Morse type potential [18,19]. The total potential energy of a single-walled CNT is expressed as

$$E = E_{stretch} + E_{angle} = \sum_i D_e \left\{ \left[1 - e^{-\beta(\Delta r_i)} \right]^2 - 1 \right\} + \frac{1}{2} \sum_j k_\theta \left(\Delta\theta_j \right)^2 \left[1 + k_{sextic} \left(\Delta\theta_j \right)^4 \right], \tag{24}$$

where D_e=0.6031 nN nm, β=26.25 nm^{-1}, k_θ=1.42 nN nm/rad^2, k_{sextic}=0.754 rad^{-4}, and Δr_i and $\Delta\theta_j$ represent bond elongation variation and bond angle variation, respectively. The stretching force resulting from bond elongation and the twisting moment resulting from bond angle variation can

be calculated by differentiating the first and the second terms of Eq. (24) with respect to bond elongation variation Δr_i and bond angle variation $\Delta\theta_j$, respectively

$$P^*\left(\Delta r_i\right) = 2\beta D_e\left[1-e^{-\beta(\Delta r_i)}\right]e^{-\beta(\Delta r_i)}, \tag{25}$$

$$M^*\left(\Delta\theta_j\right) = k_\theta\Delta\theta_j\left[1+3k_{sextic}\left(\Delta\theta_j\right)^4\right]. \tag{26}$$

Substituting Eq. (25) and Eq. (26) into the original stick-spiral model [16], the nonlinear model can be established completely. The relation between the force P and the displacement δ from nonliear model with no vdW interaction can be solved from 15 independent equations [17] (see Appendix A).

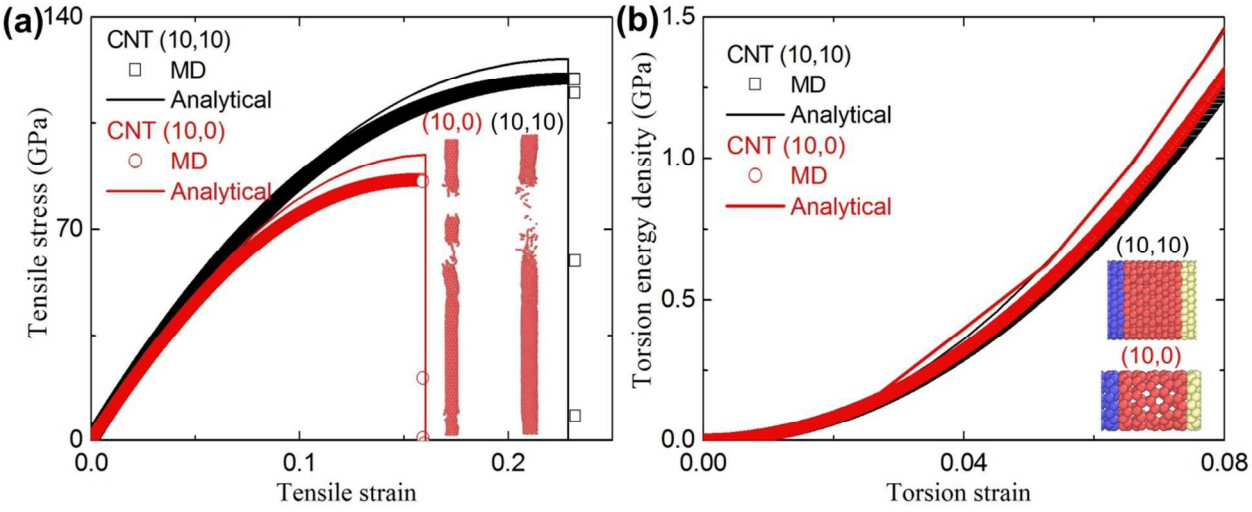

Fig. 4 (a) The tensile stress-strain curves of CNTs by Chang's analytical model and MD simulations; (b) The torsion energy density-strain curves of CNTs by our analytical model and MD simulations.

To validate the nonlinear stick-spiral model, Fig. 4 shows the stress-strain curves and the torsion energy density-strain curves of two kinds of single-walled CNTs (10,0) and (10,10) under tension and shear by Chang's nonlinear stick-spiral model and our MD simulations, respectively. All MD simulations are performed based on the Morse potential using LAMMPS [26]. Fig. 4a

shows the two CNTs (10,0) and (10,10) are both subjected to periodic boundary condition under tension at a specified low temperature (1 K) using the Nosé-Hoover thermostat and barostat, respectively. This equilibration process for 500 ps eliminates the effects of thermal vibrations before tension tests. The CNTs are subjected to strain rate 0.001/ps along the length of the CNTs by homogeneously rescaling all atoms using NPT ensemble. It can be found that the present MD results agree well with the stick-spiral model.

The torsion properties of single-walled CNTs were detailedly studied using MD simulations in previous work [27], the comparison between the MD results and the analytical model are not clear yet. To simulate the two CNTs (10,0) and (10,10) under torsion in Fig. 4, the two CNTs (10,0) and (10,10) are subjected to free boundary condition at 0 K under torsion, while a constant increment of shear strain, 10^{-4}, is applied to two rings of atoms located at the two tube ends (see Fig. 4b, in yellow and blue). The two ends are always kept as two rigid rings. The structure is optimized for each strain increment and the optimized structure is taken as the initial geometry for the next calculations. The conjugate-gradient algorithm is applied for the energy minimization, where energy and force tolerances are both 10^{-8}. It can be found that the present MD results also agree well with the stick-spiral model.

Since the vdW force $q = \frac{\partial \phi_{cicle}}{\partial h}$ between intertube walls can be obtained, the relation between the force P and the displacement δ from nonliear model with vdW interaction can be also obtained.

For (10,10) CNT, the relation between torsion stress T and torsion strain γ can be fitted by above analytical results

$$T = 471.63425\gamma\text{-}341.85006\gamma^2 + 2284.4047\gamma^3\text{-}7903.28211\gamma^4, \quad (27)$$

Substituting Eq. (2) into Eq. (27) gives

$$P=\frac{471.63425\gamma\text{-}341.85006\gamma^2+2284.4047\gamma^3\text{-}7903.28211\gamma^4}{R}, \tag{28}$$

where $\gamma=\dfrac{r_0}{\pi R\sqrt{R^2+\left(\dfrac{h+2r_0}{2\pi}\right)^2}}\delta$.

Therefore, Eq. (28) presents nonlinear force-displacement curves.

2.4 The deflection of CNC under tension using nonlinear functions of Morse potentials (including van der Waals)

Based on sections 2.2 and 2.3, the deflection of CNC with vdW force under tension using nonlinear functions of Morse potentials is considered in this section.

The stress and strain distribution can be given [17]

$$\sigma=\frac{P}{Ct}=\frac{(n+m)f_1+mf_2}{\sqrt{3}d_0t\sqrt{n^2+nm+m^2}}, \tag{29}$$

$$\varepsilon=\frac{\Delta T}{T}=\frac{d\left[(2n+m)d_1\cos\phi_1-(n-m)d_2\cos\phi_2-(2m+n)d_3\cos\phi_3\right]}{3d_0\sqrt{n^2+nm+m^2}}, \tag{30}$$

where P is an axial force, t is the thickness of the CNT (here t=3.4 Å), n and m represent the chirality of the CNT, $C=2\pi r_0$ (r_0 is the radius of the CNT), $T=3d_0(m^2+n^2+mn)^{1/2}/d_R$ [with d_R=gcd(2n+m,2m+n)] is the magnitude of the translation vector and corresponds to the length of the single-walled CNT unit cell, d_0, d_1, d_2 and d_3 are the bond length in Appendix A, respectively [17].

The nonlinear relation between above stress and strain can be fitted as follows

$$\sigma = B\varepsilon + C\varepsilon^3 + D\varepsilon^5 \quad . \tag{31}$$

where B, C and D are all constants, which can be obtained by fitting different chiral CNTs.

Substituting $\varepsilon=y/\rho$ into Eq. (31) gives

$$\sigma = \frac{By}{\rho} + \frac{Cy^3}{\rho^3} + \frac{Dy^5}{\rho^5} . \tag{32}$$

The bending moment $M = \int y\sigma dA$ can be obtained

$$M = \frac{B}{\rho}\int y^2 dA + \frac{C}{\rho^3}\int y^4 dA + \frac{D}{\rho^5}\int y^6 dA , \tag{33}$$

Substituting Eq. (33) into Eq. (14) gives δ_2.

Therefore, the displacement δ_1 and the final δ can be obtained using the same method with section 2.2.

3. Results and discussion

3.1 Results of helical CNTs

Fig. 5a shows the force-displacement curves of helical (10,10) CNT from four theoretical models. For elastic model without vdW interaction, the force-displacement curves display a linear line and are obtained from Eq. (5). The phenomenon can be found in nearly all helical macrosprings. The main reason is that the surface roughness for helical macrosprings is higher and the vdW force between the interfiber walls (normally the helical macrosprings are fibers) is considerably weak and could be neglected [25, 28, 29]. That is to say, the mechanical behavior of the helical macrospings is similar to that of the softly helical CNTs since the vdW force is neglected. For elastic model with vdW interaction, the sharply nonlinear force-displacement

relation is found at even small displacement and can be obtained from Eq. (23). If we only consider the tightly wound helical CNT as an elastic material, the vdW interaction between intertube walls dominates the nonlinear relation at even small displacement. It should be noted that the initial distance between the intertube walls is supposed to be equal to the equilibrium distance h_0 (h_0 can be determined by $\frac{\partial \phi_{cicle}}{\partial h} = 0$, see [25]). When the displacement δ is more than 6 Å (that is to say, the distance between intertube walls is $h_0+\delta$. For example, h_0=3.12 Å for two parallel (10,10) CNTs [25]), the effect of the vdW interaction on the curve disappears and then the force-displacement curve with increasing displacement is coincident with the elastic model by neglecting vdW interaction. Therefore, Hooke's law is not suitable under this condition at even small displacement, while it is correct again when the distance between intertube walls is higher than around 9 Å. It should be noted that the value of R is chosen as a constant 3 nm in order to understand the other parameters effect in this paper if no any special instruction.

To accurately predict the nonlinear properties of the softly and tightly wound helical (10,10) CNT, the force-displacement relations by considering and neglecting vdW interaction based on the nonlinear stick-spiral model with Morse potential are plotted in Fig. 5a, respectively. The sharply nonlinear force-displacement of the first nonlinear stage (That is the vdW effect zone in the circle of the inset of Fig. 5a, which is determined by vdW interaction between the intertube walls) is also found at small displacement. In particular, the maximum force P in the sharply nonlinear stage (see inset of Fig. 5a) by considering vdW interaction is almost not out of range of linear stage by neglecting vdW interaction. It indicates that the vdW interaction only affects the linear stage of the whole nonlinear force-displacement curve, while it almost has not an effect on the second nonlinear stage of the whole force-displacement curve. Actually, the competition

between vdW interaction and the nonlinear material of the spring dominates the whole nonlinear stage inclusion of the second nonlinear stage if the shear modulus of the springs is very small, and the nonlinear force-displacement curves are more complicated than Fig.5b. Fig. 5b shows the force-displacement curves for tightly helical CNTs with the same radius by considering vdW interaction. The second nonlinear stage in the force-displacement curves strongly depends on the CNT chirality, while the first nonlinear stage is weakly affected by the chirality. The reason is that the cohesive energy between two parallel CNT only depends on the radius of the CNTs from our previous work [25], which results in the high vdW force q for high radius of the CNTs. Therefore, Hooke's law can not be used to describe the force-displacement in the tightly helical CNTs, which is completely different with the helical macrosprings.

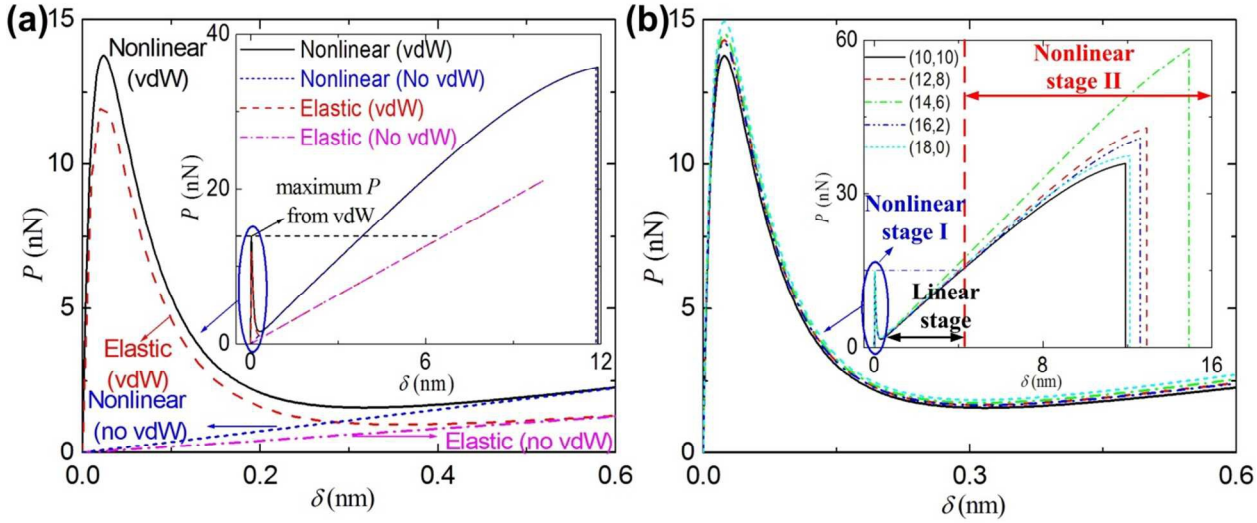

Fig. 5 (a) The force-displacement curves of (10,10) CNC from four theoretical models; (b) The force-displacement curves of same diameter CNC from nonlinear model with vdW force.

Fig. 6a shows the nonlinear force-displacement curves with different chirality and radius of the tightly helical CNTs. For a given displacement, the tensile force increases with increasing radius and chirality of the CNTs. For armchair tightly helical CNT, the tensile force increases

with increasing radius for a given displacement (see Fig. 6b). The reason is that the polar moment of inertia J and the vdW force q both increase with increasing radius of the CNTs.

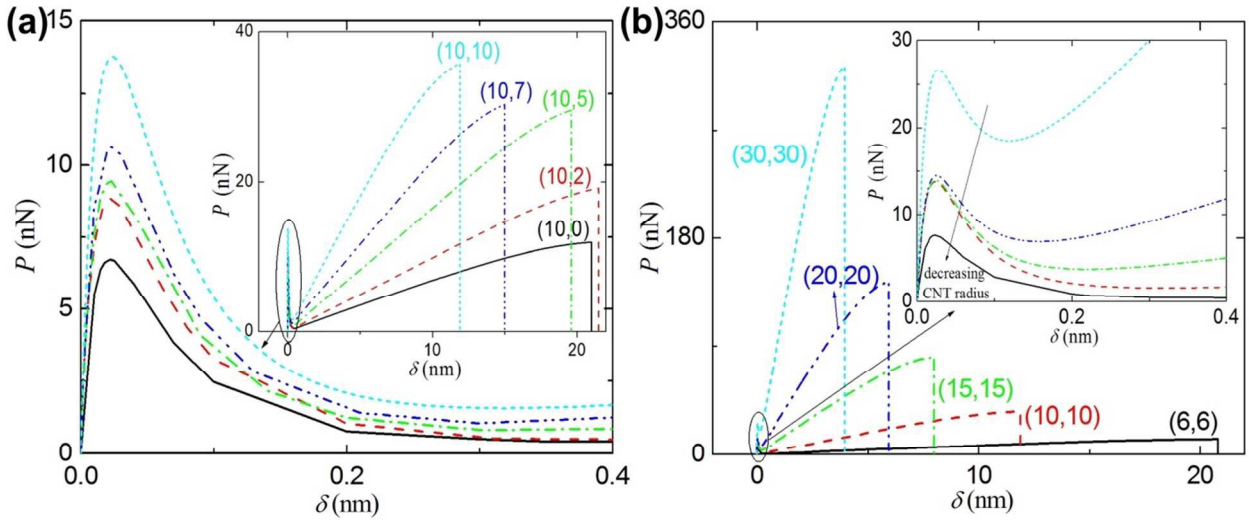

Fig.6 (a) The force-displacement curves of different chiral CNCs from nonlinear model with vdW force; (b) The force-displacement curves of different diameter CNCs from nonlinear model with vdW force.

From above analysis, Hooke's law can not be applied to the tightly helical CNT at even small displacement under tension. For softly helical CNT, it can also not be used in the two-strand or multi-strand helical CNTs when the distance between their intertube walls is close to the equilibrium distance h_0. As shown in Fig. 1c, the vdW force $q = \frac{\partial \phi_{cicle}}{\partial h}$ between the softly helical CNT1 (CNC1) and the CNC2 can be obtained from our previous work [25], and then the force-displacement curve can be given at small displacement by a superposition principle [30].

3.2 The same phenomenon in biological molecules

The α-helix structure can be often found in the biological molecules [31,32]. In order to show the same phenomenon in this structure, we build the coarse-grain (CG) MD structure of some α-helix structure in Fig. 7. All potential parameters used in this study are summarized in Table 1.

For the CG MD simulation, the helical radius R is around 2.8 nm. Each CG MD structure is generated by our code and the energy minimization is performed using the conjugate-gradient method, where energy and force tolerance are both 10^{-8} [23]. The total energy-distance (ϕ-h) and force-displacement (P-δ) curves are plotted in Fig. 7. The present analytical results agree well with our CG MD simulations. Therefore, the same phenomenon can be found not only in tightly CNCs, but also in tightly α-helix structure of biological molecules.

Table 1. Potential functions and corresponding parameters of coarse-grained method.

Interaction	Form	Parameters	
Bond	$E=\frac{1}{2}k_b\left(r_b-r_0\right)^2$	k_b=1064	kcal/mol Å^2
		r_0=1.421	Å
Angle	$E=\frac{1}{2}k_\theta\left(\theta-\theta_0\right)^2$	k_0=20	kcal/mol
		θ_0=180	degree
Non-bonded	$E=4\varepsilon\left[\left(\frac{\sigma}{r}\right)^{12}-\left(\frac{\sigma}{r}\right)^{6}\right]$	ε=0.0736	kcal/mol
		σ=3.345	Å
		r_c=30 Å	(truncation radius)

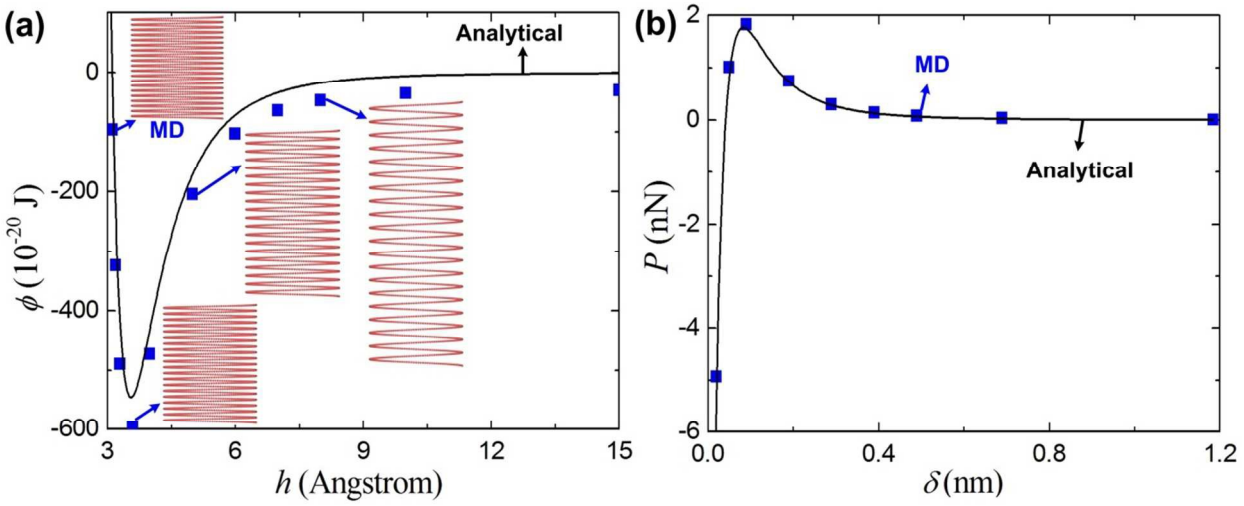

Fig. 7 The total energy-distance and force-displacement curves of α-helix structure in biological molecules under uniaxial tension using CG MD simulation.

4. Conclusion

In summary, the explicit solutions of the nonlinear force-displacement relation for tightly wound helical CNTs are obtained based on the stick-spiral model by incorporating the Morse type potential. We demonstrate that the vdW interaction between the intertube walls dominates the first nonlinear stage of the force-displacement curves. This study provides physical insights into the origins of huge nonlinearity of the helical nanosprings, nano multi-strand helical springs and α-helix structure of the biological molecules.

Acknowledgements

We gratefully acknowledge support by the National Natural Science Foundation of China (Grant No.11302084), the Fundamental Research Funds for the Central Universities (Grant No. JUSRP11529), Open Fund of Key Laboratory for Intelligent Nano Materials and Devices of the Ministry of Education (NUAA) (Grant No. INMD-2015M01) and “Thousand Youth Talents Plan”.

References:

[1] Symon K, *Mechanics*. Reading, MA: Addison-Wesley. ISBN 0-201-07392-7, (1971)

[2] Amelinckx S, Zhang XB, Bernaerts D, Zhang XF, Ivanov V, Nagy JB. A formation mechanism for catalytically grown helix -shaped graphite nanotubes. Science 1994; 265:635-9.

[3] Zhang XB, Zhang XF, Bernaerts D, Tendeloo G, Amelinckx S, Landuyt J, Ivanov V, Nagy JB, Ph L, Lucas AA. The texture of catalytically grown coil-shaped carbon nanotubules.

Europhys Lett 1994; 27:141-6.

[4] Akagi K, Tamura R, Tsukada M, Itoh S, Ihara S. Electronic structure of helically coiled cage of graphitic carbon. Phys Rev Lett 1995; 74: 2307-10.

[5] Lu W. Quantum conductance of a helically coiled carbon nanotube. Sci Technol Adv Mater 2005; 6:809-13.

[6] Volodin A, Ahlskog M, Seynaeve E, Haesendonck C, Fonseca A, Nagy JB. Imaging the elastic properties of coiled carbon nanotubes with atomic force microscopy. Phys Rev Lett 2000; 84:3342-5.

[7] Tang N, Wen J, Zhang Y, Liu F, Lin K, Du Y (2010) Helical carbon nanotubes: Catalytic particle size-dependent growth and magnetic properties. ACS Nano 2010; 4:241-50.

[8] Zhao J, Wu J, Jiang JW, Lu L, Zhang Z, Rabczuk T. Thermal conductivity of carbon nanocoils. Appl Phys Lett 2013; 103:233511.

[9] Wong BM, Ye SH. Self-assembled cyclic oligothiophene nanotubes: Electronic properties from a dispersion-corrected hybrid functional. Phys Rev B 2011; 84:075115.

[10] Hayashida T, Pan L, Nakayama Y. Mechanical and electrical properties of carbon tubule nanocoils. Physica B 2002; 323: 352-353.

[11] Zhong-can OY, Su ZB, Wang CL. Coil formation in multishell carbon nanotubes: Competition between curvature elasticity and interlayer adhesion. Phys Rev Lett 1997; 78:4055-8.

[12] Akagi K, Tamura R, Tsukada M, Itoh S, Ihara S. Electronic structure of helically coiled cage of graphitic carbon. Phys Rev Lett. 1995; 74:2307-10.

[13] Chen X, Zhang S, Dikin DA, Ding W, Ruoff RS. Mechanics of a carbon nanocoil. Nano Lett 2003; 3:1299-1304.

[14] Wu J, He J, Odegard GM, Nagao S, Zheng Q, Zhang Z. Giant stretchability and reversibility of tightly wound helical carbon nanotubes. J Am Chem Soc 2013; 135: 13775-85.

[15] Wu J, Nagao S, He JY, Zhang ZL. Nanohinge-induced plasticity in helical carbon nanotubes. Small 2013; 9:3561-66.

[16] Chang T, Gao H, Size-dependent elastic properties of a single-walled carbon nanotube via a molecular mechanics model. J Mech Phys Solids 2003; 51:1059-74.

[17] Geng J, Chang T. Nonlinear stick-spiral model for predicting mechanical behavior of single-walled carbon nanotubes. Phys Rev B 2006; 74:245428.

[18] Belytschko T, Xiao SP, Schatz GC, Ruoff R. Atomistic simulations of nanotube fracture. Phys Rev B 2002; 65:235430.

[19] Henderson RDE, Shayesteh A, Tao J, Haugen CC, Bernath PF, Le Roy RJ, J. Phys. Chem. A 2013; 117:13373-87.

[20] Ru CQ. Effect of van der Waals forces on axial buckling of a double-walled carbon nanotube. J Appl Phys 2000; 87:7227–31.

[21] Koening SP, Boddedi NG, Dunn ML, Bunch JS. Ultra-strong adhesion of graphene membranes. Nat Nanotechnol 2011; 6:543–6.

[22] Ru CQ. Axially compressed buckling of a doublewalled carbon nanotube embedded in an elastic medium. J Mech Phys Solids 2001; 49:1265–79.

[23] Zhao J, Jiang JW, Wang LF, Guo W, Rabczuk T. Coarse-grained

potentialsofsingle-walledcarbonnanotubes. J Mech Phys Solids 2014; 71:197-218.

[24] Biró LP, Lazarescu SD, Thiry PA, et al. Scanning tunneling microscopy observation of tightly wound, single-wall coiled carbon nanotubes, Europhys Lett, 2000; 50:494–500.

[25] Zhao J, Jiang JW, Jia Y, Guo W, Rabczuk T. A theoretical analysis of cohesive energy between carbon nanotubes, graphene and substrates. Carbon 2013; 57:108-19.

[26] Plimpton S. Fast parallel algorithms for short-range molecular dynamics. J Comput Phys 1995; 117:1–19.

[27] Chang T. Torsional behavior of chiral single-walled carbon nanotubes is loading direction dependent. Appl Phys Lett 2007; 90:201910.

[28] Bourauel C, Fries T, Drescher D, Plietsch R. Surface roughness of orthodontic wires via atomic force microscope, laser specular reflectance, and profilometry. Eur J Orthodont 1998; 20:79-92.

[29] Liao YS, Huang JT, Chen YH. A study to achieve a fine surface finish in wire-EDM. J Mater Process Tech 2004; 149:165-71.

[30] Lectures in Physics, Vol, 1, 1963, pg. 30-1, Addison Wesley Publishing Company Reading, Mass.

[31] Guo W, Shen R. Water Dominated Ions Stability and Conduction in NaK Channel. Biophys J 2009; 96:671.

[32] Shen R, Guo W. Ion binding properties and structure stability of the NaK channel, Biochim Biophys Acta2009;1788:1024-32.

Appendix A

We consider a (n,m) single-walled CNT subjected to an axial force P, a radial pressure σ_T, and an axial torque M_T. The nonlinear function and all equations are obtained based on the Morse potentials from Tienchong's model [17] (see Fig. A1).

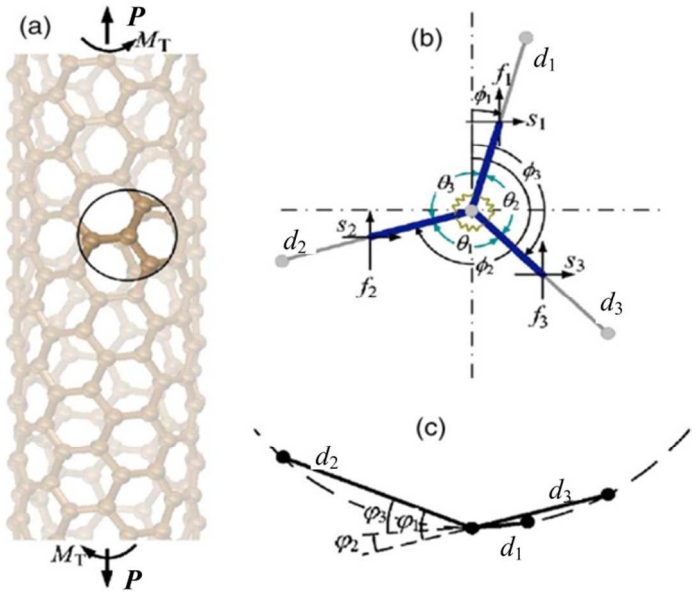

Fig. 8 (a) Global structure of a chiral nanotube; (b) Front view of local structure and schematic of the stick-spiral model; (c) Top view of local structure [17].

$$P = (n+m) f_1 + m f_2 \quad , \tag{A1}$$

$$\sigma_T = -\left[(n-m) s_1 + (2n+m) s_2\right] / (T r_0) \quad , \tag{A2}$$

$$M_T = \left[(n+m) s_1 + m s_2\right] r_0 \, , \tag{A3}$$

where r_0 is the tube radius, and f_i and s_i are forces contributed on carbon bond axial and circumferential directions.

$$f_1 + f_2 + f_3 = 0 \, , \tag{A4}$$

$$s_1 + s_2 + s_3 = 0 \, , \tag{A5}$$

$$f_i \cos\phi_i + s_i \sin\phi_i = P^*\left(\Delta d_i\right),\ (i=1,2,3) \tag{A6}$$

$$\frac{d_i}{2}\left(f_i \sin\phi_i - s_i \cos\phi_i\right) = M^*\left(\Delta\theta_i\right)\cos\omega_{ij} + M^*\left(\Delta\theta_k\right)\cos\omega_{ik},\ (i,j,k=1,2,3;\ i\neq j\neq k) \tag{A7}$$

where ω_{ij}, the torsion angle between the plan though d_i parallel to the nanotube axis and the plan of θ_j can be calculated by

$$\cos\omega_{ij} = \left(\cos\phi_i \sin\phi_k \cos\varphi_j - \sin\phi_i \cos\phi_k\right)/\sin\theta_j \quad ,\ (i,j,k=1,2,3;\ i\neq j\neq k) \tag{A8}$$

$$\Delta\theta_i = -\left(\Delta\phi_j \cos\omega_{ji} + \Delta\phi_k \cos\omega_{ki}\right) \quad ,\ (i,j,k=1,2,3;\ i\neq j\neq k) \tag{A9}$$

$$\Delta\left[md_1\cos\phi_1 - (n+m)d_2\cos\phi_2 + nd_3\cos\phi_3\right] = 0, \tag{A10}$$

$$\gamma = \frac{\Delta\left[(2n+m)d_1\sin\phi_1 - (n-m)d_2\sin\phi_2 - (2m+n)d_3\sin\phi_3\right]}{3d_0\sqrt{n^2+nm+m^2}}, \tag{A11}$$

We note here that P, σ_T, and M_T are applied external forces. Once these forces are given, the present problem is solvable. For example, letting σ_T=0 and M_T=0, with a stepwise increase in the axial strain, the mechanical behavior of a SWCNT under axial loading can be obtained via the non-linear stick-spiral model.